Characterizing Alzheimer's Disease Biomarker Cascade Through Non-linear Mixed Effect Models

Zhuojun $\mathrm{Tang}^{1,\dagger},$ Yuxin $\mathrm{Zhu}^{2,4,5,\dagger},$ and Zheyu $\mathrm{Wang}^{3,5,*}$

¹Department of Industrial and Systems Engineering, North Carolina State University, Raleigh, NC 27606, U.S.A.

²Armstrong Institute for Patient Safety and Quality, Johns Hopkins University, Baltimore, MD 21202, U.S.A.

³Division of Quantitative Sciences, Sidney Kimmel Comprehensive Cancer Center,

Johns Hopkins University, Baltimore, MD 21205, U.S.A.

⁴Department of Neurology, Johns Hopkins School of Medicine, Baltimore, MD 21205, U.S.A.

⁵Department of Biostatistics, Johns Hopkins Bloomberg School of Public Health, Baltimore, MD 21205, U.S.A.

(†These authors have equal contributions.)

*email: wangzy@jhu.edu (corresponding author)

Summary: Alzheimer's Disease (AD) research has shifted to focus on biomarker trajectories and their potential use in understanding the underlying AD-related pathological process. A conceptual framework was proposed in modern AD research, which hypothesized biomarker cascades as a result of underlying AD pathology. In this paper, we leverage the idea of biomarker cascades and develop methods that use a non-linear mixed effect model to depict AD biomarker trajectories as a function of the latent AD disease progression. We tailored our methods to address a number of real-data challenges present in BIOCARD and ADNI studies. We illustrate the proposed methods with simulation studies as well as analysis results on the BIOCARD and ADNI data showing the ordering of various biomarkers from the CSF, MRI, and cognitive domains. We investigated cascading patterns of AD biomarkers in these datasets and presented prediction results for individual-level profiles over time. These findings highlight the potential of the conceptual biomarker cascade framework to be leveraged for diagnoses and monitoring. KEY WORDS: non-linear mixed effect regression, disease prediction, biomarker monitoring

1. Introduction

Research on Alzheimer's Disease (AD) has shifted its focus to early stages of AD, during which cognitive impairment has yet started or is just starting, and intervention is the most likely to be effective. Researchers are especially interested in understanding AD biomarkers in relation to underlying AD pathological stages, and have hypothesized that a preclinical AD stage exists. During this hypothesized preclinical AD stage, patients experience deterioration in brain deposition biomarkers but may not exhibit any clinical signs of cognitive decline that warrant a diagnosis. This preclinical AD stage is followed by the mild cognitive impairment (MCI) stage, during which the neurodegenerative process and earliest onset of cognitive symptoms begin, and then by the dementia stage, during which cognitive impairment is present in multiple domains and results in a further loss of cognitive functions.

Jack and colleagues proposed an influential conceptual framework for AD staging and AD biomarkers (Jack Jr et al., 2010, 2013b,a), assuming that: 1) the underlying AD pathological process is continuous and clinical decline happens gradually; 2) AD biomarkers become abnormal and reach a plateau in a temporal order, possibly following sigmoid-shaped trajectories; and 3) the AD biomarker trajectories are important to be studied in relation to the underlying disease process and can potentially be used for the effective identification of preclinical and MCI stages of AD. This conceptual model, commonly referred to as the Jack model, provides a unique opportunity for models to be built on AD studies to inform AD staging and to elucidate the ordering of AD biomarker cascades. AD studies with biomarker measurements collected when participants were cognitively normal (CN) without any sign of clinical symptoms are especially valuable, because they might contain information on biomarker profiles during the preclinical stage of AD. AD biomarker data collected in early stages of AD, combined with further longitudinal observations, could potentially further reveal how AD biomarkers change during various AD stages.

In this paper, we consider the modeling of longitudinally observed AD biomarkers by leveraging the conceptual Jack model. Specifically, we assume that a continuous latent disease process affects the multifaceted and longitudinal biomarkers through logistic link functions that depict the S-shape of biomarker progression trajectories, which we have informally referred to as "biomarker cascades". We further implement these models on the BIOCARD and ADNI study data, which we discuss in more details in Section 2. The proposed model and analyses are intend to provide data driven information to help characterizing 1) the temporal ordering of biomarker cascades in relation to the AD progression, 2) the multifaceted profile of biomarkers at various stages of AD progression, and 3) disease progression based on biomarker data without relying on clinical diagnoses, which has the potential of unveiling new insights by going beyond diagnosis-based analyses that are biased towards existing practice.

In addition to formulating a statistical model based on the conceptual framework described by Jack and colleague, we attempt to address unique challenges that often arise in current AD studies with longitudinal biomarker measurements due to the decades long preclinical and clinical stages of AD as well as limitation in assessment frequency and time. One advantage of some current AD longitudinal studies is that they have long follow-up starting from when participants were CN. Meanwhile, biomarker measurements are limited due to cost and sometimes the intrusive nature of sample collection procedures. The concerns for the relatively small number of measurements are elevated, considering the slow disease progression and the necessary long follow-up duration to observe the progression. Observing limited number of longitudinal biomarker measurements may pose a risk for weak estimability of certain model parameters, especially those characterizing the plateau height of the sigmoid curves. Further techniques that utilizes external or additional information that may inform the model need to be developed and studied.

The remainder of this paper is structured as follows. In Section 3, we present methods for modeling biomarkers as a function of the underlying disease process, including discussion on general models and special strategies addressing real-world data challenges. In Section 4, we present simulation studies illustrating empirical validity and performance of proposed methods under various less-than-ideal settings similar to those in the real data. Analysis results in two real-world AD longitudinal follow-up study datasets are presented in Section 5, followed by discussions in Section 6.

2. BIOCARD and ADNI study data

Our methods are motivated by the need to understand biomarker cascades and particularly with considerations in two datasets: 1) the BIOCARD: Predictors of Cognitive Decline Among Normal Individuals (BIOCARD) and 2) the subset of CN participants at baseline in Alzheimer's Disease Neuroimaging Initiative (ADNI) study data. We consider these two datasets because they contain longitudinal data for participants followed from when they were CN at baseline, have considerably long follow-up duration, and are similar in protocols for biomarker measurements.

The BIOCARD study is a longitudinal and observational study initiated at the National Institute of Health in 1995. At baseline, 349 cognitively normal individuals that were primarily middle-aged and had a first-degree relative with dementia were recruited and followed by NIH (1995 to 2005) and Johns Hopkins University (2009 to present). During the active study duration, clinical assessments with cognitive tests were done annually for study participants. Magnetic resonance imaging (MRI), cerebrospinal fluid (CSF), and blood specimens were collected biannually. Study participants also receive consensus diagnoses at annual clinical visits, categorized as either cognitively normal (CN), mild cognitive impairment (MCI), or dementia. For individuals that receive a diagnosis of dementia, the age at clinical symptom onset is determined based on the clinical dementia rating (CDR) interview. Individuals in

the BIOCARD study have been followed for an average of 15.5 years, creating a precious data source for understanding biomarker and disease progression trajectories.

The ADNI study is a multi-center observational study initiated in 2003. The ADNI study recruited participants across the spectrum of AD from the categories of CN, MCI, and AD, defined based on memory criteria, the Mini-Mental State Examination (MMSE), and CDR score. We include in our analyses 2115 participants that were CN at baseline and followed for an average of 3.6 years (range: 0-15 years). Subjects were evaluated at 6 to 12 month intervals for 2 to 3 years, depending on the clinical diagnosis at baseline. Clinical, imaging, genetic, and biospecimen data were collected. To make analysis results and interpretations comparable between the BIOCARD and ADNI data, our analysis focus on the subset of ADNI participants that were CN at baseline.

3. Methodology

3.1 Non-linear mixed effects model for biomarker progression

We consider a set of observations for N independent subjects and K distinct biomarker measurements that are measured over time for these subjects. Let Y_{ijk} denote the value of the kth biomarker for subject i at the jth visit, where i = 1, ..., N, $j = 1, ..., J_i$, $k \in \kappa_{ij} \subset \{1, ..., K\}$. Denote by D_{ij} the underlying AD-related disease progression process, which we also refer to as the AD disease progression for simplicity, of subject i at time t_{ij} .

Following the description in Jack Jr et al. (2010), we model biomarker levels to be a sigmoid-shaped function of the AD disease progression, with possible effects from other covariates as follows:

$$Y_{ijk} = \boldsymbol{X}_{ij}^T \boldsymbol{\beta}_k + f_k(D_{ij}; \boldsymbol{\gamma}_k) + \epsilon_{ijk}$$
 (1)

where X_{ij} is a p-dimensional vector denoting the ith patient's covariate information (including an intercept) at the jth visit, and β_k is the p-dimensional biomarker-specific linear

coefficient vector. Here, f_k is a predetermined function parametrized by vector γ_k , describing S-shaped biomarker trajectories along disease progression. In addition to correlation through the shared risk score, we allow biomarkers collected at the same visit to correlate with each other through the error term ϵ_{ijk} . This is particularly relevant when multiple biomarkers are collected from the same domain of interest (e.g., Digit Symbol Substitution Test and Logical Memory delayed recall from the cognitive tests), as there are likely correlations due to shared measurement construct in addition to the shared underlying disease. Specifically, let $\epsilon_{ij} = (\epsilon_{ij1}, \dots, \epsilon_{ijK})^{\mathsf{T}}$. We assume that $\epsilon_{ij} \sim N(0, \Sigma_{\epsilon})$, where $\Sigma_{\epsilon} = \Sigma(\sigma_1, \dots, \sigma_K, \phi^{\mathsf{T}})$ is the variance-covariance matrix parametrized by the marginal variance parameters $\sigma_1, \dots, \sigma_K$ and a vector ϕ depicting the correlation structure.

We select link function f_k 's that reflect the biomedical hypothesis on biomarker progression. Without loss of generality, we also assume that the biomarkers have been transformed such that higher biomarker values are associated with greater AD disease progressions, indicating further disease progression. We use a logistic function to model $f_k(D_{ij}; \gamma_k)$ as follows:

$$f_k(D_{ij}; \boldsymbol{\gamma}_k) = \frac{\gamma_{k1}}{1 + \exp\left\{-\gamma_{k2}(D_{ij} - \gamma_{k3})\right\}}, \text{ where } \gamma_{k1}, \gamma_{k2} > 0.$$
 (2)

The logistic function covers a range of sigmoid-shapes similar to the curves proposed in the Jack model. The parameters also have intuitive interpretations: γ_{k1} is the maximum height of the curve, representing the highest value of abnormality for the kth biomarker during the AD cascade that we are interested in; the parameter γ_{k2} reflects the steepness of the sigmoid curve, representing the speed of biomarker level change during AD progression; and γ_{k3} is the reflection point of the sigmoid curve, which can be considered as the location when biomarker changes are halfway towards the highest abnormality values of interest, providing one way to determine the ordering of biomarker deterioration.

The relationship between covariates and AD disease progression d_{ij} is modeled as

$$D_{ij} = \mathbf{Z}_{ij}^{\mathsf{T}} \boldsymbol{\alpha} + \delta_{ij} \tag{3}$$

where $\mathbf{Z}_{ij} \in \mathbb{R}^q$ denote covariates including demographic variables such as age and risk factors such as ApoE-4 carrier status, and $\boldsymbol{\alpha} \in \mathbb{R}^q$ are coefficients. For model identifiability, we fix the location and scale of the latent variable D_{ij} by removing the intercept term in $\boldsymbol{\alpha}$ and setting the variance of δ_{ij} to be one.

For the remainder of this paper, we will use lowercase notations to denote the data realization that corresponds to random variables.

3.2 Practical modeling considerations for data structures

We estimate the proposed model through likelihood estimation. Let $\Phi_q(\mu, \Sigma)$ denote the distribution function of a q-dimensional multivariate normal distribution with mean μ and variance-covariance matrix Σ , and let $e_{\kappa} \in \mathbb{R}^{K}$ denote a vector with ones in elements indexed by index set κ and zeros elsewhere. Furthermore, let $\boldsymbol{Y}_{ij} = (Y_{ij1}, \dots, Y_{ijK})^\mathsf{T}$, $\boldsymbol{\beta} = (\boldsymbol{\beta}_1^\mathsf{T}, \dots, \boldsymbol{\beta}_K^\mathsf{T})^\mathsf{T}, \; \boldsymbol{\theta} = (\boldsymbol{\beta}_1^\mathsf{T}, \dots, \boldsymbol{\beta}_K^\mathsf{T}, \boldsymbol{\gamma}_1^\mathsf{T}, \dots, \boldsymbol{\gamma}_K^\mathsf{T}, \sigma_1, \dots, \sigma_K, \boldsymbol{\phi}^\mathsf{T})^\mathsf{T}, \; f.(D_{ij}; \boldsymbol{\gamma}_1, \dots, \boldsymbol{\gamma}_K) = (\boldsymbol{\beta}_1^\mathsf{T}, \dots, \boldsymbol{\beta}_K^\mathsf{T}, \boldsymbol{\gamma}_1^\mathsf{T}, \dots, \boldsymbol{\gamma}_K^\mathsf{T}, \sigma_1, \dots, \sigma_K, \boldsymbol{\phi}^\mathsf{T})^\mathsf{T}, \; f.(D_{ij}; \boldsymbol{\gamma}_1, \dots, \boldsymbol{\gamma}_K) = (\boldsymbol{\beta}_1^\mathsf{T}, \dots, \boldsymbol{\beta}_K^\mathsf{T}, \boldsymbol{\gamma}_1^\mathsf{T}, \dots, \boldsymbol{\gamma}_K^\mathsf{T}, \sigma_1, \dots, \sigma_K, \boldsymbol{\phi}^\mathsf{T})^\mathsf{T}, \; f.(D_{ij}; \boldsymbol{\gamma}_1, \dots, \boldsymbol{\gamma}_K) = (\boldsymbol{\beta}_1^\mathsf{T}, \dots, \boldsymbol{\beta}_K^\mathsf{T}, \boldsymbol{\gamma}_1^\mathsf{T}, \dots, \boldsymbol{\gamma}_K^\mathsf{T}, \boldsymbol{\gamma}_1^\mathsf{T}, \dots, \boldsymbol{\gamma}_K^\mathsf{T}, \boldsymbol{\gamma}_1^\mathsf{T}, \dots, \boldsymbol{\gamma}_K^\mathsf{T}, \boldsymbol{\gamma}_K^\mathsf{T}, \boldsymbol{\gamma}_1^\mathsf{T}, \dots, \boldsymbol{\gamma}_K^\mathsf{T}, \boldsymbol{\gamma}_K^\mathsf{T}, \boldsymbol{\gamma}_K^\mathsf{T}, \boldsymbol{\gamma}_K^\mathsf{T}, \boldsymbol{\gamma}_K^\mathsf{T}, \boldsymbol{\gamma}_K^\mathsf{T}, \boldsymbol{\gamma}_K^\mathsf{T}, \dots, \boldsymbol{\gamma}_K^\mathsf{T}, \boldsymbol{\gamma}_$ $\{f_1(D_{ij}; \boldsymbol{\gamma}_1), \dots, f_K(D_{ij}; \boldsymbol{\gamma}_K)\}^\mathsf{T}$, \odot denote the element-wise multiplication, and \cdot denote the matrix multiplication. In contrast with vector \boldsymbol{Y}_{ij} containing all biomarker values including those not observed, we denote by $oldsymbol{Y}_{ij,\kappa_{ij}}$ the observed biomarker vector containing elements index by $k \in \kappa_{ij}$. Longitudinal observations of biomarkers are subject to two layers of missingness: 1) a clinical visit can be entirely missing because the participants did not come in as scheduled; 2) at a observed clinical visit, subset of biomarkers can be scheduled not to be collected during that visit and thus missing. We assume that both clinical visits (first layer) and biomarker measurements (second layer) are subject to missingness at random (MAR). The MAR assumption for biomarker measurements is likely to hold because they are administratively scheduled independent of patient background and disease progression. The MAR assumption for clinical visits is a stronger assumption, but still likely to hold given collected covariates. The likelihood of the biomarker progression model can then be written as

$$L(\boldsymbol{\theta}, \boldsymbol{\alpha}) = \prod_{i=1}^{N} \prod_{j=1}^{J_{i}} \int_{\mathbb{R}} f_{\boldsymbol{Y}_{ij,\kappa_{ij}}|D_{ij}}(\boldsymbol{y}_{ij,\kappa_{ij}}|d, \boldsymbol{x}_{ij}, \boldsymbol{\theta}) \cdot f_{D_{ij}}(d|\boldsymbol{z}_{ij}, \boldsymbol{\alpha}) \, \mathrm{d}d$$

$$= \prod_{i=1}^{N} \prod_{j=1}^{J_{i}} \int_{\mathbb{R}} \int_{\mathbb{R}^{|\kappa_{ij}|}} d\Phi_{|\kappa_{ij}|} \left[\{ y_{ij} - \boldsymbol{x}_{ij}^{\mathsf{T}} \boldsymbol{\beta} - f_{\cdot}(d; \boldsymbol{\gamma}_{1}, \dots, \boldsymbol{\gamma}_{K}) \} \odot e_{\kappa_{ij}}, \right]$$

$$e_{\kappa_{ij}} \cdot \boldsymbol{\Sigma}_{\epsilon} \cdot e_{\kappa_{ij}}^{\mathsf{T}} d\Phi_{1}(d - \boldsymbol{z}_{ij}^{\mathsf{T}} \boldsymbol{\alpha}, 1),$$

$$(4)$$

and parameter estimates can be obtained through likelihood maximization.

Meanwhile, the estimation procedure in our real data application still requires a few special considerations. These include degenerative cases of the logistic function, determining biomarker abnormality range when data do not cover the full longitudinal span of disease progression, and improving computational efficiency regarding correlation parameters, which we discuss below.

3.2.1 Determining the range of biomarker progression given limited longitudinal spans.

Given the slow progression nature of AD, observation of biomarkers starting from when participants were CN often do not temporally span over the entirety from CN to AD. This data structure leads to model estimability issues under the Jack model and thus creates challenges for quantitatively studying the hypothesized biomarker cascades. Specifically, "late-development" biomarkers, such as cognitive tests, are unlikely to have enough observations during the plateau of the sigmoid curves, and the height parameters can be weakly estimable, or the estimates of these parameters can have large bias and variability.

For these "late-development" biomarkers, we borrow from empirical knowledge to inform the corresponding γ_{k1} values. Specifically, we average biomarker values measured at "cognitively normal" visits, where the biomarker values are believed to be in the initial flat stage, and at "dementia" visits, where the biomarker values are believed to have plateaued. We consider a visit to be a "cognitively normal" visit if it is the baseline visit for an individual who has stayed cognitively normal throughout the entire follow-up period, and consider a

visit to be a "dementia" visit if a clinical diagnosis of dementia is given at or before that visit. We then use the difference between the two averages, with appropriate standardization, as the known value for γ_{k1} . The empirically derived γ_{k1} values are subject to noise, and we investigate the performance of proposed methods in Section 4 by conducting estimation given randomly perturbed γ_{k1} values. We implement the described procedures for all biomarkers: we determine values γ_{k1} based on observed biomarker levels and plug them in during model estimation as if they were known.

3.2.2 Degenerative cases of biomarker progression trajectory. The logistic function used in equation (2) include degenerative cases that fall outside the hypothesized sigmoid shape when γ_{k2} is close to zero or infinity. Specifically, when $\gamma_{k2} \to 0$, $f_k(d_{ij}; \gamma_k) \to \gamma_{k1}/2$, indicating that the biomarker level is a horizontal line and unrelated to disease progression. When $\gamma_{k2} \to \infty$, we have $f_k(d_{ij}; \gamma_k) \to \mathbb{I}(d_{ij} < \gamma_{k3}) \cdot 0 + \mathbb{I}(d_{ij} > \gamma_{k3}) \cdot \gamma_{k1}$, which is a step-function with singularity at $d_{ij} = \gamma_{k3}$, indicating that the biomarker level remains constant over time except for an acute jump when disease progression reaches a certain point. Scientifically, neither degenerative case is well-supported by evidence in the medical literature. Although theoretically, these degenerative cases do not require special handling in ideal situations when we have large sample sizes and large numbers of longitudinal observations, in real data where sample sizes and longitudinal follow-ups are limited, estimation stability is a concern. Pre-hoc exclusion of unrealistic degenerative cases can be leveraged to improve model fit and extraction of information from real data.

To implement this, we restrict the γ_{k2} parameters to be between 0 and 10, and add a likelihood penalty term that penalizes extreme values that are close to the 0 and 10 boundaries. Specifically, we choose to minimize $-\log L + \lambda \cdot \sum_{k=1}^{K} n_k^{1/4} \cdot g(\gamma_{k2})$, where $g(\gamma_{k2}) = \log(\gamma_{k2}/10) + \log(1 - \gamma_{k2}/10)$. The penalty function $g(\gamma_{k2})$ has the property that it imposes large penalties for values that are close to the boundaries (we have $\partial g(\gamma_{k2})/\partial \gamma_{k2} \to \infty$ when

 $\gamma_{k2} \to 0^+$ or $\gamma_{k2} \to 10^-$) and moderate penalties for values that are away from the boundaries. We included the scaling term $n_k^{1/4}$ to account for the different sample sizes of biomarkers, while ensuring that the effect of the penalty terms is not driven by the more frequently measured biomarkers. The rate of 1/4 also ensures that the asymptotic normality of estimator is unchanged. We choose the tuning parameter λ through 10-fold cross-validation, and details are discussed in Sections 4 and 5.

3.2.3 Correlation parameter in variance-covariance matrices. We assume independence across time (visits), that is, we have $Cor(\epsilon_{ijk}, \epsilon_{ij'k'}) = 0$, representing independent biomarker measurement errors conditional on underlying disease and covariates across time, and $Cor(\sigma_{ij}, \sigma_{ij'}) = 0$ for any $j \neq j'$, representing temporal independence in disease within a participant. The former is a standard independent error assumption. The latter is an assumption made to take advantage of the fast computational speed of a simplified model while maintaining estimation accuracy. As shown by simulation studies in Section 4, ignoring possible disease temporal correlation within a participant minimally hurts estimation under realistic data structures. Meanwhile, this simplifying model assumption allows us to use the exact optimization in combination with Gauss-Hermite quadrature approximation when maximizing the penalized likelihood. The use of Gauss-Hermite quadrature approximation greatly improves computational speed, in comparison with the use of approximation-based optimization approaches that are necessary for models allowing disease temporal correlations to be nonzero. Detailed discussions on the exact and approximation-based optimization approaches and the Gauss-Hermite quadrature approximation are provided in Section 3.3.1.

3.3 Estimation

3.3.1 Point estimation through maximum likelihood. Due to nonlinearity in NLME models, the likelihood typically does not have closed-form expressions. Multiple approximation-based and exact optimization approaches have been proposed for the estimation of the NLME

model. Approximation-based optimization often used for estimating NLME models uses first-order Taylor expansions or Laplace's methods (Lindstrom and Bates, 1990; Wolfinger, 1993) and can be quite time-efficient. However, the time efficiency comes at the cost of considerable approximation errors, especially when individuals have sparse data or when the variability of the random effects is large (Vonesh, 1996). Exact optimization approaches, on the other hand, can be computationally faster under appropriate model assumptions while controlling approximation errors, and therefore more applicable for our model estimation. We adopt the Newton-Raphson (NR) optimization algorithm in this work. Further numerical approximation methods for computing the likelihood need to be used in combination with NR algorithm. Commonly used numerical approximations include Monte Carlo and Gauss-Hermite quadrature (GQ). Monte-Carlo NR algorithms work for random effects with any dimensions and any distributions. However, they are not specialized to be computationally fast under our specific model assumptions that d_{ij} 's are independent across j's. A more tailored numerical approximation is the GQ, which significantly reduces our computational time when used with the NR algorithm.

Now we present the details of GQNR algorithm. Equivalent to maximizing the likelihood, we solve the following score equations of the likelihood:

$$H_1(oldsymbol{x},oldsymbol{y},oldsymbol{z},oldsymbol{ heta},oldsymbol{x}) = \sum_{i=1}^N \sum_{j=1}^{J_i} \mathbb{E}_{D_{ij}|oldsymbol{Y}_{ij,\kappa_{ij}},(oldsymbol{ heta},oldsymbol{lpha})} \Big[rac{\partial \log f_{oldsymbol{Y}_{ij,\kappa_{ij}}|D_{ij}}(oldsymbol{y}_{ij,\kappa_{ij}}|D_{ij},oldsymbol{x}_{ij},oldsymbol{ heta})}{\partial oldsymbol{ heta}} \Big| oldsymbol{y}_{ij,\kappa_{ij}} \Big] = oldsymbol{0}, \ H_2(oldsymbol{x},oldsymbol{y},oldsymbol{z},oldsymbol{ heta},oldsymbol{lpha}}) = \sum_{i=1}^N \sum_{j=1}^{J_i} \mathbb{E}_{D_{ij}|oldsymbol{Y}_{ij,\kappa_{ij}},(oldsymbol{ heta},oldsymbol{lpha})} \Big[rac{\partial \log f_{D_{ij}}(oldsymbol{D}_{ij}|oldsymbol{z}_{ij},oldsymbol{lpha})}{\partial oldsymbol{lpha}} \Big| oldsymbol{y}_{ij,\kappa_{ij}} \Big] = oldsymbol{0}.$$

Updates of the parameter estimates are then made marginally using the Newton-Raphson algorithm. Denote by $\boldsymbol{\theta}^{(m)}$ and $\boldsymbol{\alpha}^{(m)}$ the parameter estimates at the *m*th step of Newton-

Raphson iterative algorithm (m = 1, 2, ...).

$$\boldsymbol{\theta}^{(m+1)} = \boldsymbol{\theta}^{(m)} - \left(\frac{\partial H_1}{\partial \boldsymbol{\theta}^T}(\boldsymbol{x}, \boldsymbol{y}, \boldsymbol{z}, \boldsymbol{\theta}^{(m)}, \boldsymbol{\alpha}^{(m)})\right)^{-1} H_1(\boldsymbol{x}, \boldsymbol{y}, \boldsymbol{z}, \boldsymbol{\theta}^{(m)}, \boldsymbol{\alpha}^{(m)}),$$

$$\boldsymbol{\alpha}^{(m+1)} = \boldsymbol{\alpha}^{(m)} - \left(\frac{\partial H_2}{\partial \boldsymbol{\alpha}^T}(\boldsymbol{x}, \boldsymbol{y}, \boldsymbol{z}, \boldsymbol{\theta}^{(m)}, \boldsymbol{\alpha}^{(m)})\right)^{-1} H_2(\boldsymbol{x}, \boldsymbol{y}, \boldsymbol{z}, \boldsymbol{\theta}^{(m)}, \boldsymbol{\alpha}^{(m)}).$$
(5)

An interesting observation is that implementing the Newton-Raphson update is marginally equivalent to the EM algorithm update with a one-step Newton-Raphson in the M-step (Wang, 2007).

During the iterative updating of the parameter estimates, the closed-form expressions

$$\sum_{i=1}^{N} \sum_{j=1}^{J_i} \mathbb{E}_{D_{ij}|\mathbf{Y}_{ij,\kappa_{ij}},(\boldsymbol{\theta},\boldsymbol{\alpha})=(\boldsymbol{\theta}^{(m)},\boldsymbol{\alpha}^{(m)})} [h(D_{ij})|\mathbf{y}_{ij,\kappa_{ij}}],$$
(6)

in (5) are unavailable, where $h(D_{ij})$ is some function of D_{ij} . In our case, specific forms of $h(D_{ij})$ are

$$\begin{aligned} & \left\{ \partial \log f_{\boldsymbol{Y}_{ij,\kappa_{ij}}|D_{ij}}(\boldsymbol{y}_{ij,\kappa_{ij}}|D_{ij},\boldsymbol{x}_{ij},\boldsymbol{\theta})/\partial \boldsymbol{\theta} \right\} \Big|_{\boldsymbol{\theta}=\boldsymbol{\theta}^{(m)}}, \\ & \left\{ \partial^{2} \log f_{\boldsymbol{Y}_{ij,\kappa_{ij}}|D_{ij}}(\boldsymbol{y}_{ij,\kappa_{ij}}|D_{ij},\boldsymbol{x}_{ij},\boldsymbol{\theta})/\partial \boldsymbol{\theta}^{\mathsf{T}} \partial \boldsymbol{\theta} \right\} \Big|_{\boldsymbol{\theta}=\boldsymbol{\theta}^{(m)}}, \\ & \left\{ \partial \log f_{D_{ij}}(D_{ij}|\boldsymbol{z}_{ij},\boldsymbol{\alpha})/\partial \boldsymbol{\alpha} \right\} \Big|_{\boldsymbol{\alpha}=\boldsymbol{\alpha}^{(m)}}, \\ & \left\{ \partial^{2} \log f_{D_{ij}}(D_{ij}|\boldsymbol{z}_{ij},\boldsymbol{\alpha})/\partial \boldsymbol{\alpha}^{\mathsf{T}} \partial \boldsymbol{\alpha} \right\} \Big|_{\boldsymbol{\alpha}=\boldsymbol{\alpha}^{(m)}}, \end{aligned}$$

at the *m*th step, respectively. To compute (6), we use the Gauss-Hermite quadrature approximation—an approximation to $\mathbb{E}_{D_{ij}|\mathbf{Y}_{ij,\kappa_{ij}}}[g(D_{ij})|\mathbf{y}_{ij,\kappa_{ij}}]$ via Q-point Gauss-Hermite quadrature

$$\mathbb{E}_{D_{ij}|\mathbf{Y}_{ij,\kappa_{ij}}}[g(D_{ij})|\mathbf{y}_{ij,\kappa_{ij}}] = \frac{\int_{-\infty}^{\infty} g(d) f_{\mathbf{Y}_{ij,\kappa_{ij}}|D_{ij}}(\mathbf{y}_{ij,\kappa_{ij}}|d,\mathbf{x}_{ij},\boldsymbol{\theta}) f_{D_{ij}}(d|\mathbf{z}_{ij},\boldsymbol{\alpha}) \,\mathrm{d}d}{\int_{-\infty}^{\infty} f_{\mathbf{Y}_{ij,\kappa_{ij}}|D_{ij}}(\mathbf{y}_{ij,\kappa_{ij}}|d,\mathbf{x}_{ij},\boldsymbol{\theta}) f_{D_{ij}}(d|\mathbf{z}_{ij},\boldsymbol{\alpha}) \,\mathrm{d}d}$$

$$\approx \frac{\sum_{q=1}^{Q} w_q \cdot g(2^{1/2}b_q + \mathbf{z}_{ij}^{\mathsf{T}}\boldsymbol{\alpha}) f_{\mathbf{Y}_{ij,\kappa_{ij}}|D_{ij}}(\mathbf{y}_{ij,\kappa_{ij}}|d = 2^{1/2}b_q + \mathbf{z}_{ij}^{\mathsf{T}}\boldsymbol{\alpha},\mathbf{x}_{ij},\boldsymbol{\theta})}{\sum_{q=1}^{Q} w_q \cdot f_{\mathbf{Y}_{ij,\kappa_{ij}}|D_{ij}}(\mathbf{y}_{ij,\kappa_{ij}}|d = 2^{1/2}b_q + \mathbf{z}_{ij}^{\mathsf{T}}\boldsymbol{\alpha},\mathbf{x}_{ij},\boldsymbol{\theta})},$$

$$(7)$$

where b_q is the q-th root of the physicists' version of the Hermite polynomial, and w_q is the associated weight.

In practical implementation, the GQNR algorithm can be inefficient for high-dimensional integrals, so we use the Monte Carlo Newton-Raphson (MCNR) algorithm proposed by

McCulloch (McCulloch, 1997) to obtain initial values, under further simplified model assumptions. Specifically, we first assume that no correlation exists in biomarker measurement errors and use MCNR to obtain estimation, which is in turn used as starting values for running the GQNR algorithm for the full model.

3.3.2 Variance-covariance estimation through Louis' formula. The variance-covariance matrix of the coefficient estimators can be estimated by the inverse of the observed information matrix and calculated using the Louis' formula (Louis, 1982) as

$$I(\widehat{\boldsymbol{\theta}}, \widehat{\boldsymbol{\alpha}}) = -I^{c}(\widehat{\boldsymbol{\theta}}, \widehat{\boldsymbol{\alpha}}) - \sum_{i=1}^{n} \mathbb{E} \left[S_{i}(\widehat{\boldsymbol{\theta}}, \widehat{\boldsymbol{\alpha}}) S_{i}^{\mathsf{T}}(\widehat{\boldsymbol{\theta}}, \widehat{\boldsymbol{\alpha}}) \middle| \boldsymbol{y}_{i}, \widehat{\boldsymbol{\theta}}, \widehat{\boldsymbol{\alpha}} \right] + \sum_{i=1}^{n} \mathbb{E} \left[S_{i}(\widehat{\boldsymbol{\theta}}, \widehat{\boldsymbol{\alpha}}) \middle| \boldsymbol{y}_{i}, \widehat{\boldsymbol{\theta}}, \widehat{\boldsymbol{\alpha}} \right] \mathbb{E} \left[S_{i}^{\mathsf{T}}(\widehat{\boldsymbol{\theta}}, \widehat{\boldsymbol{\alpha}}) \middle| \boldsymbol{y}_{i}, \widehat{\boldsymbol{\theta}}, \widehat{\boldsymbol{\alpha}} \right],$$

where

$$S_{i}(\boldsymbol{\theta}, \boldsymbol{\alpha}) = \left(\sum_{j=1}^{J_{i}} \partial \log f_{\boldsymbol{Y}_{ij,\kappa_{ij}}|D_{ij}}(\boldsymbol{y}_{ij,\kappa_{ij}}|D_{ij},\boldsymbol{x}_{ij},\boldsymbol{\theta})/\partial \boldsymbol{\theta}, \sum_{j=1}^{J_{i}} \partial \log f_{D_{ij}}(D_{ij}|\boldsymbol{z}_{ij},\boldsymbol{\alpha})/\partial \boldsymbol{\alpha}\right),$$

$$I_{\boldsymbol{\theta}}^{c}(\boldsymbol{\theta}) = \sum_{i=1}^{n} \sum_{j=1}^{J_{i}} \mathbb{E}\left[\left\{\partial^{2} \log f_{\boldsymbol{Y}_{ij,\kappa_{ij}}|D_{ij}}(\boldsymbol{y}_{ij,\kappa_{ij}}|D_{ij},\boldsymbol{x}_{ij},\boldsymbol{\theta})/\partial \boldsymbol{\theta}^{\mathsf{T}} \partial \boldsymbol{\theta}\right\} \middle| \boldsymbol{y}_{i},\boldsymbol{\theta}\right],$$

$$I_{\boldsymbol{\alpha}}^{c}(\boldsymbol{\alpha}) = \sum_{i=1}^{n} \sum_{j=1}^{J_{i}} \mathbb{E}\left[\partial^{2} \log f_{D_{ij}}(D_{ij}|\boldsymbol{z}_{ij},\boldsymbol{\alpha})/\partial \boldsymbol{\alpha}^{\mathsf{T}} \partial \boldsymbol{\alpha}\right],$$

$$I^{c}(\boldsymbol{\theta},\boldsymbol{\alpha}) = \begin{pmatrix} I_{\boldsymbol{\theta}}^{c}(\boldsymbol{\theta}) & \mathbf{0} \\ \mathbf{0} & I_{\boldsymbol{\alpha}}^{c}(\boldsymbol{\alpha}) \end{pmatrix}.$$

Louis' formula was developed for computing the observed information matrix in the EM algorithm. However, it is applicable to our estimation because the Newton-Raphson algorithm described in Section 3.3.1 is essentially equivalent to an EM algorithm and all components needed for applying the Louis' formula are calculated in the last step of Newton-Raphson update. To address the possible numerical instability resulting in the information matrix being singular or negative-definite and non-invertible, we applied the generalized Cholesky decomposition, as implemented in R package matrixcalc, to the observed information

matrix. A generalized inversion of matrix can then be computed and used as the estimator for $Var(\widehat{\theta}, \widehat{\alpha})$.

3.4 Estimation, prediction, and monitoring of disease and biomarker trajectories

With the model-informed relationship between the underlying disease and observed biomarker,
we can use observed biomarker information from a patient to infer and project their underlying disease (D_i) at the current visit as well as at a future time. We can also use biomarker
distribution among patients with similar underlying diseases to detect potential deviation
from "normal" biomarker trajectories and alert potential unusual deterioration. We discuss
these prediction and monitoring tools below.

We first introduce some notations for this section. Let $\hat{\boldsymbol{\theta}} = (\hat{\boldsymbol{\beta}}_1^\mathsf{T}, \dots, \hat{\boldsymbol{\beta}}_K^\mathsf{T}, \hat{\gamma}_1^\mathsf{T}, \dots, \hat{\boldsymbol{\gamma}}_K^\mathsf{T}, \hat{\sigma}_1, \dots, \hat{\sigma}_K, \hat{\boldsymbol{\phi}}^\mathsf{T})^\mathsf{T}$ and $\hat{\boldsymbol{\alpha}}$ denote the parameter estimates. Denote by $\boldsymbol{Z}_{ij} = \boldsymbol{z}$ and $\boldsymbol{X}_{ij} = \boldsymbol{x}$ the covariates collected at time point t_0 when the jth visit occurs for the ith participant, and by $\boldsymbol{z}(t)$ and $\boldsymbol{x}(t)$ the corresponding covariates at a general time point t (we then have $\boldsymbol{z}(t_0) = \boldsymbol{z}$ and $\boldsymbol{x}(t_0) = \boldsymbol{x}$). In our practical application, all components of \boldsymbol{X}_{ij} and \boldsymbol{Z}_{ij} are time-invariant variables such as ApoE-4 carrier status, gender, and years of education, excepting for an age or time variable, so $\boldsymbol{x}(t)$ values are known for both time points when visits occur and future time point. In addition to covariates that will be incorporated in prediction and monitoring, we predict the AD disease progression at specific visit using the set of observed biomarkers \boldsymbol{y}_{κ} for subscript set $\kappa \subset \left\{1,\dots,K\right\}$. We also consider the extrapolated biomarker values $\tilde{\boldsymbol{y}}_{\kappa}(t)$ from \boldsymbol{y}_{κ} , which is measured at t_0 , to a future time point t. The extrapolated biomarker value is calculated by assuming that the biomarker deteriorates according to the age effect described in equation (1), that is, $\tilde{\boldsymbol{y}}_{\kappa}(t) = \boldsymbol{y}_{\kappa}(t_0) + \left\{\boldsymbol{x}(t) - \boldsymbol{x}(t_0)\right\}^{\mathsf{T}} \hat{\boldsymbol{\beta}}_{\kappa}$ where $\hat{\boldsymbol{\beta}}_{\kappa}$ is a matrix with rows of estimated regression coefficients. As a special case, we have $\tilde{\boldsymbol{y}}_{\kappa}(t_0) = \boldsymbol{y}_{\kappa}(t_0)$.

3.4.1 Disease progression estimation and prediction. We synthesize information on covariates and biomarkers to predict the underlying disease progression, either for observed

visits given covariates and observed biomarkers, or for future visits given covariates and extrapolated biomarkers accounting for natural aging effects. Conditional on covariates $X_{ij} = x(t)$ and $Z_{ij} = z(t)$, we have estimated the joint probability density function for biomarker vector $Y_{ij\kappa}$ containing observed measurements (missing measurements are integrated out) and disease status as

$$\widehat{f}_{\boldsymbol{Y}_{ij\kappa},D_{ij}|\boldsymbol{X}_{ij},\boldsymbol{Z}_{ij}}(\boldsymbol{y}_{\kappa},d|\boldsymbol{X}_{ij}=\boldsymbol{x}(t),\boldsymbol{Z}_{ij}=\boldsymbol{z}(t))$$

$$=\phi_{\kappa}\left[\left\{\boldsymbol{y}_{\cdot}-\boldsymbol{x}(t)^{\mathsf{T}}\widehat{\boldsymbol{\beta}}-f(d;\widehat{\boldsymbol{\gamma}}_{k})\right\}\odot\boldsymbol{e}_{\kappa}\cdot\left\{\boldsymbol{e}_{\kappa}\cdot\widehat{\boldsymbol{\Sigma}}\cdot\boldsymbol{e}_{\kappa}^{\mathsf{T}}\right\}^{1/2}\right]\cdot\phi_{1}\left\{d-\boldsymbol{z}(t)^{T}\boldsymbol{\alpha}\right\},$$
(8)

Based on this joint distribution, we can then derive conditional distribution of disease given covariates $\boldsymbol{x}(t)$ and $\boldsymbol{z}(t)$ and observed or extrapolated biomarker values $\widetilde{\boldsymbol{y}}_{\kappa}(t)$ as

$$\widehat{f}_{D_{ij}|\boldsymbol{Y}_{ij,\kappa},\boldsymbol{X}_{ij},\boldsymbol{Z}_{ij}}(d|\widetilde{\boldsymbol{y}}_{\kappa}(t),\boldsymbol{x}(t),\boldsymbol{z}(t)) = \frac{\widehat{f}_{\boldsymbol{Y}_{ij,\kappa},D_{ij}|\boldsymbol{X}_{ij},\boldsymbol{Z}_{ij}}(\widetilde{\boldsymbol{y}}_{\kappa}(t),d|\boldsymbol{x}(t),\boldsymbol{z}(t))}{\widehat{f}_{\boldsymbol{Y}_{ij,\kappa}|\boldsymbol{X}_{ij},\boldsymbol{Z}_{ij}}(\widetilde{\boldsymbol{y}}_{\kappa}(t)|\boldsymbol{x}(t),\boldsymbol{z}(t))},$$

from which we can simulate Monte Carlo samples $\left\{d^{(\ell)}\right\}_{\ell=1}^{L}$. Having obtained the resampled $\left\{d^{(\ell)}\right\}_{\ell=1}^{L}$, we use the mean as the predicted value of disease, the asymptotic variance of which can be computed by simulating from the asymptotic distribution of $(\widehat{\boldsymbol{\theta}}, \widehat{\boldsymbol{\alpha}})$ and utilizing formula (7). We also use a% and (100-a)% quantiles as lower and upper bounds of the (100-2a)% prediction interval.

The projected future AD progressions, along with their corresponding intervals, would serve as benchmarks for comparison when biomarkers for future visits become available. Specifically, we propose to compare predicted value of D_{ij} given $\boldsymbol{x}(t)$, $\boldsymbol{z}(t)$ and observed $\boldsymbol{y}_{\kappa}(t)$ to that of D_{ij} given $\boldsymbol{x}(t)$, $\boldsymbol{z}(t)$ and extrapolated $\tilde{\boldsymbol{y}}_{\kappa}(t)$: if predicted AD disease progression given actual observed biomarkers are much higher than the projected AD disease progression, it constitutes evidence supporting that the AD disease progression in addition to normal aging exists. We present relevant analysis results on BIOCARD and ADNI datasets in more details in Section 5.

3.4.2 Monitoring biomarker deterioration. We propose a system for biomarker monitoring based on the predicted underlying disease status and our biomarker model. The goal is

to detect potential biomarker values that are worse than expected, such as a particular area shown in MRI or a particular cognitive function, that appear to be worse than patients with similar underlying disease. The monitoring of biomarkers complements the one-dimensional information given in the predicted AD progressions, in that it reflects the multi-faceted view of AD progression as discussed in Sperling et al. (2011) and potentially signaling the start of accelerated worsening of the underlying disease.

Suppose that we are given biomarker and covariate information at t_0 , and we predict the underlying AD disease progression to be the conditional expectation denoted by d_0 . At the time of visit where covariates and some biomarkers are observed, we are interested in the distribution of biomarker values conditional on the disease risk score d_0 and the observed covariate profile, and where the observed biomarkers fall within that distribution. We have similar research interest in understanding biomarker distribution given covariate profile and some appropriately chosen underlying AD disease progression at a future time point (t_1) . For these future time points, we specifically consider the extrapolated AD disease progression following the aging trajectory, calculated as $\tilde{d}(t_1) = d_0 + \{z(t_1) - z(t_0)\}^{\mathsf{T}} \hat{\alpha}$.

For either a visit time point t_0 at which biomarker measurements are collected or a future time point t_1 at which no data is yet observed, we predict the biomarker distributions given covariates and the predicted or extrapolated AD disease risk score $\tilde{d}(t)$ ($t = t_0, t_1$), following approaches similar to those discussed in Section 3.4.1. The predicted distributions are then used as the benchmark for comparison with observed biomarker values. Specifically, we predict y_{ijk} for given $D_{ij} = \tilde{d}(t)$ by simulating, for $\ell = 1, \ldots, L$, the error term $\epsilon_{ij}^{(\ell)} = (\epsilon_{ij1}^{(\ell)}, \ldots, \epsilon_{ijK}^{(\ell)})$ from K-dimensional multivariate normal distribution with mean zero and variance-covariance matrix $\hat{\Sigma}$, and then compute $y_{ijk}^{(\ell)}\{\tilde{d}(t)\} = \mathbf{X}_{ij}^{\mathsf{T}}\hat{\boldsymbol{\beta}}_k + f_k\{\tilde{d}(t); \hat{\boldsymbol{\gamma}}_k\} + \epsilon_{ijk}^{(\ell)}$ as a function of d. The mean of the computed $\{y_{ijk}^{(\ell)}\{\tilde{d}(t)\}\}_{\ell=1}^{L}$ and the a% and (100-a)% quantiles then serve to establish thresholds for monitoring biomarker deterioration or improvement.

4. Simulations

We conduct simulation studies to investigate the finite-sample performance of the proposed estimator under less than ideal settings that are often present in real data. Specifically, we consider three scenarios to respectively study the performance of the proposed estimator when: 1) the sample size is relatively small but more longitudinal visits are available, and the estimated height parameters are subject to noise; 2) the sample size is relatively large but fewer longitudinal visits are available, and the estimated height parameters are subject to noise; 3) when temporal correlations exist between disease status within the same participant, but the model is misspecified.

We simulate observations from the model

$$Y_{ijk} = 1 + X_{ij1} + X_{ij2} + \frac{3}{1 + \exp\{-3(D_{ij} - \gamma_{k3})\}} + \epsilon_{ijk},$$
$$D_{ij} = X_{ij1} + X_{ij2} + \delta_{ij},$$

for k=1,2,3,4, where δ_{ij} follows standard normal distribution as required for model identifiability, $(\epsilon_{ij1}, \epsilon_{ij2}, \epsilon_{ij3}, \epsilon_{ij4})$ follows mean-zero multivariate normal distribution with variance of ones and correlation of zeros except for the correlation between ϵ_{ij1} and ϵ_{ij2} . We assume that the correlation between ϵ_{ij1} and ϵ_{ij2} is 0.7 to emulate the correlation between biomarkers coming from the same domain, in addition to the shared disease and covariate effect. We simulate covariate X_{ij1} from the standard normal distribution and covariate X_{ij2} as a balanced binary variable. We also take $\gamma_{k3}=3-k$ to represent the varied cascading locations: the biomarkers indexed by k=1,2 deteriorate late, emulating biomarkers coming from the cognitive domain; the biomarkers indexed by k=3,4 deteriorate early, emulating biomarkers coming from the MRI or CSF domains. The simulation model described, compared to the general form of the model specified by (1), (2), and (3), has taken $X_{ij} = Z_{ij} = (X_{ij1}, X_{ij2}), \alpha = (1,1)^{\mathsf{T}}, \beta = (1,1,1)^{\mathsf{T}}$, and $\gamma_{k1} = \gamma_{k2} = 3$.

We also generate two layers of missingness to imitate what we have in real data. We

generate data for N participants and J_i regularly spaced visits at time points $0, 1, \ldots, J_i - 1$. Each of the visits is then randomly (completely at random) assigned a missingness status with 30% probability of missing. Given that a visit is observed, we then generate random missingness of each biomarker: we let biomarkers be missing with zero probability (i.e., all are observed) for k = 1, 2, with 0.2 probability for k = 3, and with 0.4 probability for k = 4. For each subject, this amounts to an average of $0.7 \cdot J_i$ biomarker observations for k = 1, 2, $0.56 \cdot J_i$ for k = 3, and $0.42 \cdot J_i$ for k = 4.

In addition to these shared settings, we vary data generation mechanisms slightly for each of the three scenarios that we consider. In the first and second scenarios, we plug in a noise-perturbed (mean zero normal error with a standard deviation of 0.05) version of the true γ_{k1} values for estimation, while varying the sample size N and the number of visits J_i . In the first scenario, we take N=300 and $J_i=20$ (an average of 14 visits for k = 1, 2, 11.2 visits for k = 3, and 8.4 visits for k = 4), similar to the BIOCARD data structure; in the second scenario, we take N=800 and $J_i=15$ (an average of 10.5 visits for k = 1, 2, 8.4 visits for k = 3, and 6.3 visits for k = 4), similar to the ADNI data structure. The first two scenarios are designed for the investigation of estimator performance under realistic situations where plugged-in γ_{k1} values are subject to errors because they are derived from data and with approximations. We also consider a third simulation scenario as a modification of the first scenario, where temporal correlation exists but estimation is done under the misspecified model assuming temporal independence. Specifically, we generate errors δ_{ij} such that $Cor(\delta_{ij}, \delta_{ij'}) = 0.3^{|j-j'|}$. We carry out the estimation strategy described in Section 3.3, which maximizes a penalized likelihood. The tuning parameter for penalty is chosen through 10-fold cross validations.

We conduct simulations for 1000 replications under each scenario and report biases, empirical standard errors (ESE) and mean standard errors (MSE) in Table 1. For the first and

second scenarios, we can observe from simulation results that, in the presence of slightly perturbed γ_{k1} 's, biases are small, MSEs are close to ESEs, and 95% confidence interval coverage probability is close to the theoretical value. Simulation results for the third scenario suggest that the estimation remains valid even when the model is misspecified in assuming no correlation across visits. We do observe poorer finite performance in β_{k1} (one of the biomarker model regression coefficient) and γ_{k2} (progression curve slope parameter) for biomarkers that deteriorate late indexed by k = 1, 2. We also observe poorer performance in β_{k0} and β_{k1} for some of the biomarkers that deteriorate early, indexed by k = 3, 4. These results suggest the importance of predetermining a good estimate of the height parameters (γ_{k1}), and noise in the predetermined height parameter values might affect early biomarkers (e.g., CSF biomarkers) more than the late biomarkers (e.g., cognitive tests).

[Table 1 about here.]

5. Analyses on biomarker cascading model using the BIOCARD and ADNI data

In this section, we present details of the real data analysis process, and analysis and prediction results. We first discuss details of the data merging procedures for the BIOCARD and ADNI data separately. We then present the model specifications including covariates and biomarker correlation structures. After detailing the analytic approach, we present estimation results in Tables 2, 3, and Figure 1, and showcase prediction and monitoring methods with Figure 2.

To create datasets that are suitable for analyses, we merge biomarker measurements to harmonize the irregular visit times. Out of considerations for model misspecification as discussed in Section 3.2, we use cognitive visits as "anchoring visits" to which we merge other biomarker measurements. Specifically, for the BIOCARD data, we use cognitive visit

dates as the anchoring visit date, whereas for the ADNI data, we generate annually spaced dates starting from baseline as cognitive visit dates, to merge various cognitive test scores collected over a few days for the same visit. Next, for both the BIOCARD and ADNI data, we merge MRI and CSF biomarker measurements taken within two-year (730 days) windows on each side of that cognitive visit to the visit date.

When multiple biomarker measurements exist within the measurement window, we only merge the temporally closest measurement, and we allow one biomarker measurement to be used multiple times in merging. We allow a two-sided two-year window for merging the MRI and CSF biomarker measurements because these biomarkers are less often collected due to high cost but are considered to be reasonably stable within a two-year window.

We consider the modeling of the following biomarkers in data analyses: the Digit Symbol Substitution Test (DSST) score, the Mini-Mental State Exam (MMSE) score, and the Logical Memory delayed recall (LM) score from the cognitive test domain; entorhi nal cortex (EC) thickness, EC volume, hippocampal (HIPPO) volume, medial temporal lobe composite score (MTL), which is constructed based on volumes of HIPPO, EC and amygdala. Further, we model the Spatial Pattern of Abnormality for Recognition of Early Alzheimer's Disease score (SPARE-AD; included in the model for BIOCARD only) (Davatzikos et al., 2009; Weintraub et al., 2012) from the MRI domain; and $A\beta$ ($A\beta42/40$ ratio for the BIOCARD, $A\beta$ for the ADNI), PTau and Ttau from the CSF domain. We include in the biomarker model (1) age, gender, and years of education as covariates, and we include in the AD disease progression model (3) age and ApoE-4 carrier status as covariates. We assume temporal independence across visits, allow biomarkers model errors to have correlation within the same domain, and assume independence of biomarker errors from different domains. Specifically, we specify the error correlation structure according to preliminary data analyses on the

marginal correlations between markers. Detailed correlation structures are shown in Figures 1.A3 and 1.B3.

As discussed in Section 3.2, we have a few additional data considerations during estimation. First, we predetermine the values of γ_{k1} from observed biomarker values and plug them in during model estimation as if they were known. Specifically, we aggregate biomarker values at what we consider to be typical CN and AD visits, compute the means at these two types of visits respectively, and use the properly transformed differences as the predetermined γ_{k1} 's. We consider baseline visits of participants that remained CN throughout to be typical CN visits, and visits of the first AD diagnosis to be typical AD visits. Second, we incorporate the penalty term as described in Section 3.2.2, choosing the tuning parameter λ from 16 candidate values between 10^{-2} and 10^{2} according to 10-fold cross validations. The tuning parameter is chosen to be $10^{0.3} \approx 2$ for the BIOCARD data and $10^{0.6} \approx 4$ for the ADNI data. Coefficient estimates with 95% confidence intervals are presented in Table 2 for BIOCARD and in Table 3 for ADNI. We further illustrate in Figure 1 the estimated biomarker progression curves and biomarker cascade ordering as shown by the γ_{k3} parameters. After the model estimation, we carry out prediction of the disease and biomarker trajectories as described in Section 3.4, and we show results in Figure 2 as an illustration.

We observe from analysis results, especially the biomarker progression curves as shown in Figure 1, that the BIOCARD and ADNI data exhibit similar patterns: biomarkers from the CSF domain are the first to deteriorate, followed by those from the MRI domain and then the cognitive domain. Specially, within the CSF domain, $A\beta$ is consistently shown to progress first. Ordering of biomarkers within the MRI and cognitive domains respectively are less clear due to wide confidence intervals. Meanwhile, it is interesting to observe that biomarker progression curves have crossovers, which implies that the biomarker cascade ordering could be different depending on the location of biomarker abnormality (y-axis). Also of note, the

Characterizing Alzheimer's Disease Biomarker Cascade Through Non-linear Mixed Effect Models

21

disease scales in BIOCARD and ADNI data, as reflected by the x-axes in Figures 1.A1 and

1.B1, are different because both biomarkers and covariates (standardized to have mean zero

and standard deviation one if continuous) are on different scales.

To illustrate disease prediction and biomarker monitoring procedures discussed in Section

3.4, we show in Figure 2.A the estimated disease trajectories (given covariates and available

biomarkers) as participants age, and in Figure 2.B the estimated disease trajectories pre-

sented on the timescale relative to the time of onset, for participants who had onset of clinical

symptoms. In Figure 2.C, we show an example of a biomarker and disease monitoring panel

using longitudinal data from one patient, with the red dotted vertical line separating past

visits, at which we have collected biomarker information, and the future. For each biomarker,

we present the predicted biomarker trajectory given covariates and estimated disease for past

visits or projected disease for the future, accompanied by dotted lines showing the upper

and lower boundaries of 50% prediction intervals. We also plot observed biomarker values

as discrete points, and the relative positions of observed values and the prediction interval

boundaries highlight the multi-faceted biomarker profile of the patient when compared to a

similar population in terms of age, gender, education, ApoE-4 carrier status, and underlying

disease status. In addition to the biomarkers, we also show the estimated and projected

disease trajectory of that patient, accompanied by a 95% CI (the narrower interval) and a

50% prediction interval (the wider interval).

[Table 2 about here.]

[Figure 1 about here.]

[Figure 2 about here.]

6. Discussion

This paper proposes a parametric non-linear mixed effect model to characterize Jack and his colleagues' biomarker cascade hypothesis for AD. Our proposed methods taken into considerations the unique data structures often seen in observational longitudinal studies of AD, such as the BIOCARD and ADNI studies. These data make it possible to build statistical models of biomarker cascading and understanding them: a crucial step in improving our understanding of how AD progresses, especially in the preclinical stages. Through simulation studies, we investigate the finite-sample behavior of the proposed methods under realistic settings where various challenges exist. Furthermore, we implemented and illustrated the proposed estimation and prediction approaches on the BIOCARD and ADNI data. The analysis results suggest that CSF biomarkers tend to worsen first, followed by MRI and cognitive biomarkers, which are patterns consistent with evidence in the literature and existing hypotheses. We note that these results are obtained under parametric model assumptions and need to be interpreted with this limitation.

In this study, we have made significant contributions towards understanding biomarker cascades and the relationship between biomarkers and AD progression. Our work has potentially important implications for clinical practice and future research related to diagnosing and predicting AD, especially preclinical AD. However, there are a few limitations that should be considered. One limitation is that we adopt a parametric model. Semi-parametric or non-parametric modeling approaches may provide a more flexible and reliable way to study the complex relationships between biomarkers and disease progression. Another limitation is that we analyzed the BIOCARD and ADNI data separately, which may limit the generalizability of our results. Future research could explore methods to harmonize and combine both datasets to increase the sample size, improve the precision of estimates, and potentially increase the generalizability of the results. Overall, our work provided some insights for

biomarker cascades and how biomarkers can be leveraged in predicting disease progression, laying a foundation for future research in this area.

Acknowledgements

The authors' efforts are supported by NIA grant R01AG068002. The authors would also like to thank Dr. Shannon L. Cole for his invaluable contributions in revising and editing this manuscript, which greatly improved its quality.

References

- Davatzikos, C., Xu, F., An, Y., Fan, Y., and Resnick, S. M. (2009). Longitudinal progression of alzheimer's-like patterns of atrophy in normal older adults: the spare-ad index. *Brain* **132**, 2026–2035.
- Jack Jr, C. R., Knopman, D. S., Jagust, W. J., Petersen, R. C., Weiner, M. W., Aisen, P. S., Shaw, L. M., Vemuri, P., Wiste, H. J., Weigand, S. D., et al. (2013a). Tracking pathophysiological processes in alzheimer's disease: an updated hypothetical model of dynamic biomarkers. The Lancet Neurology 12, 207–216.
- Jack Jr, C. R., Knopman, D. S., Jagust, W. J., Petersen, R. C., Weiner, M. W., Aisen, P. S., Shaw, L. M., Vemuri, P., Wiste, H. J., Weigand, S. D., et al. (2013b). Update on hypothetical model of alzheimer's disease biomarkers. *Lancet neurology* 12, 207.
- Jack Jr, C. R., Knopman, D. S., Jagust, W. J., Shaw, L. M., Aisen, P. S., Weiner, M. W., Petersen, R. C., and Trojanowski, J. Q. (2010). Hypothetical model of dynamic biomarkers of the alzheimer's pathological cascade. *The Lancet Neurology* 9, 119–128.
- Lindstrom, M. J. and Bates, D. M. (1990). Nonlinear mixed effects models for repeated measures data. *Biometrics* pages 673–687.
- Louis, T. A. (1982). Finding the observed information matrix when using the em algorithm.

 Journal of the Royal Statistical Society: Series B (Methodological) 44, 226–233.

- McCulloch, C. E. (1997). Maximum likelihood algorithms for generalized linear mixed models. *Journal of the American statistical Association* **92**, 162–170.
- Sperling, R. A., Aisen, P. S., Beckett, L. A., Bennett, D. A., Craft, S., Fagan, A. M., Iwatsubo, T., Jack Jr, C. R., Kaye, J., Montine, T. J., et al. (2011). Toward defining the preclinical stages of alzheimer's disease: Recommendations from the national institute on aging-alzheimer's association workgroups on diagnostic guidelines for alzheimer's disease. *Alzheimer's & dementia* 7, 280–292.
- Vonesh, E. F. (1996). A note on the use of laplace's approximation for nonlinear mixed-effects models. *Biometrika* 83, 447–452.
- Wang, J. (2007). Em algorithms for nonlinear mixed effects models. *Computational statistics*& data analysis 51, 3244–3256.
- Weintraub, D., Dietz, N., Duda, J. E., Wolk, D. A., Doshi, J., Xie, S. X., Davatzikos, C., Clark, C. M., and Siderowf, A. (2012). Alzheimer's disease pattern of brain atrophy predicts cognitive decline in parkinson's disease. *Brain* 135, 170–180.
- Wolfinger, R. (1993). Laplace's approximation for nonlinear mixed models. *Biometrika* **80**, 791–795.

Received xx 2023. Revised xx 2023. Accepted xx 2023.

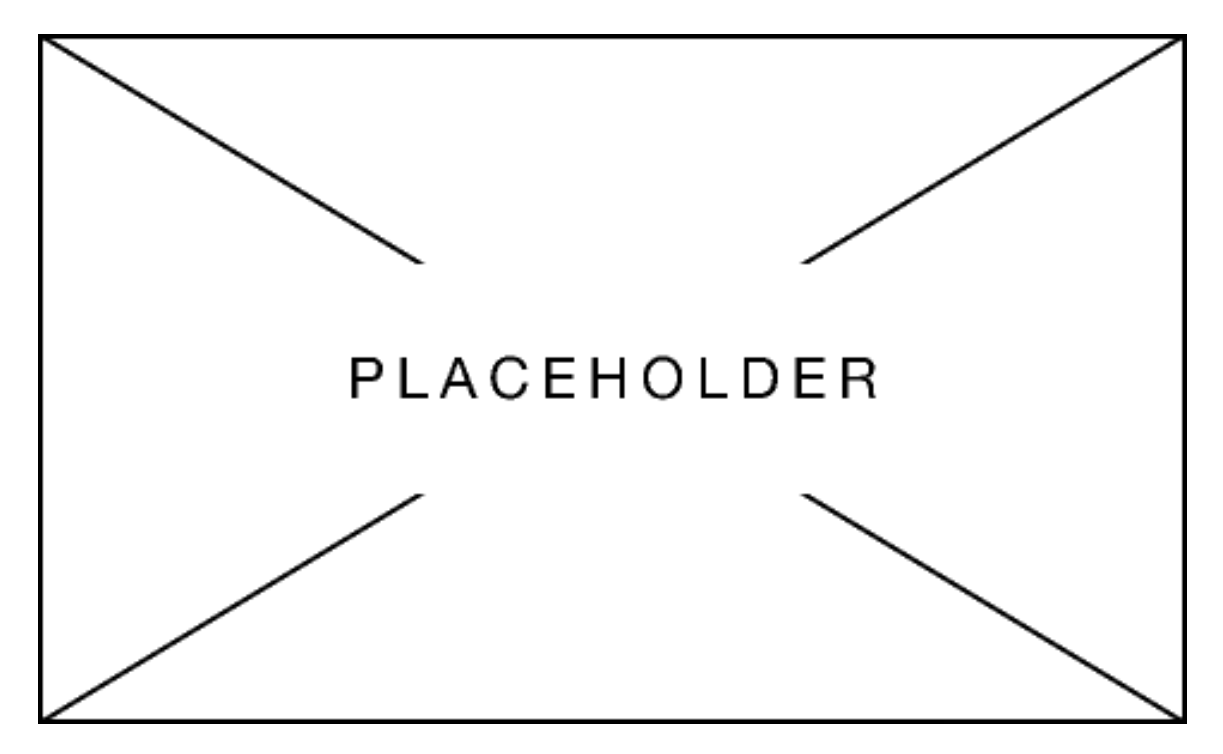


Figure 1: Analysis results for BIOCARD and ADNI data. A1-A3 show results for BIOCARD; B1-B3 show results for ADNI. A1 and B1 illustrate the estimated biomarker progression curves $f_k(d)$; A2 and B2 illustrate the ordering as shown by the estimated location parameter γ_{k3} ; A3 and B3 illustrate the correlation structures for biomarker error terms.

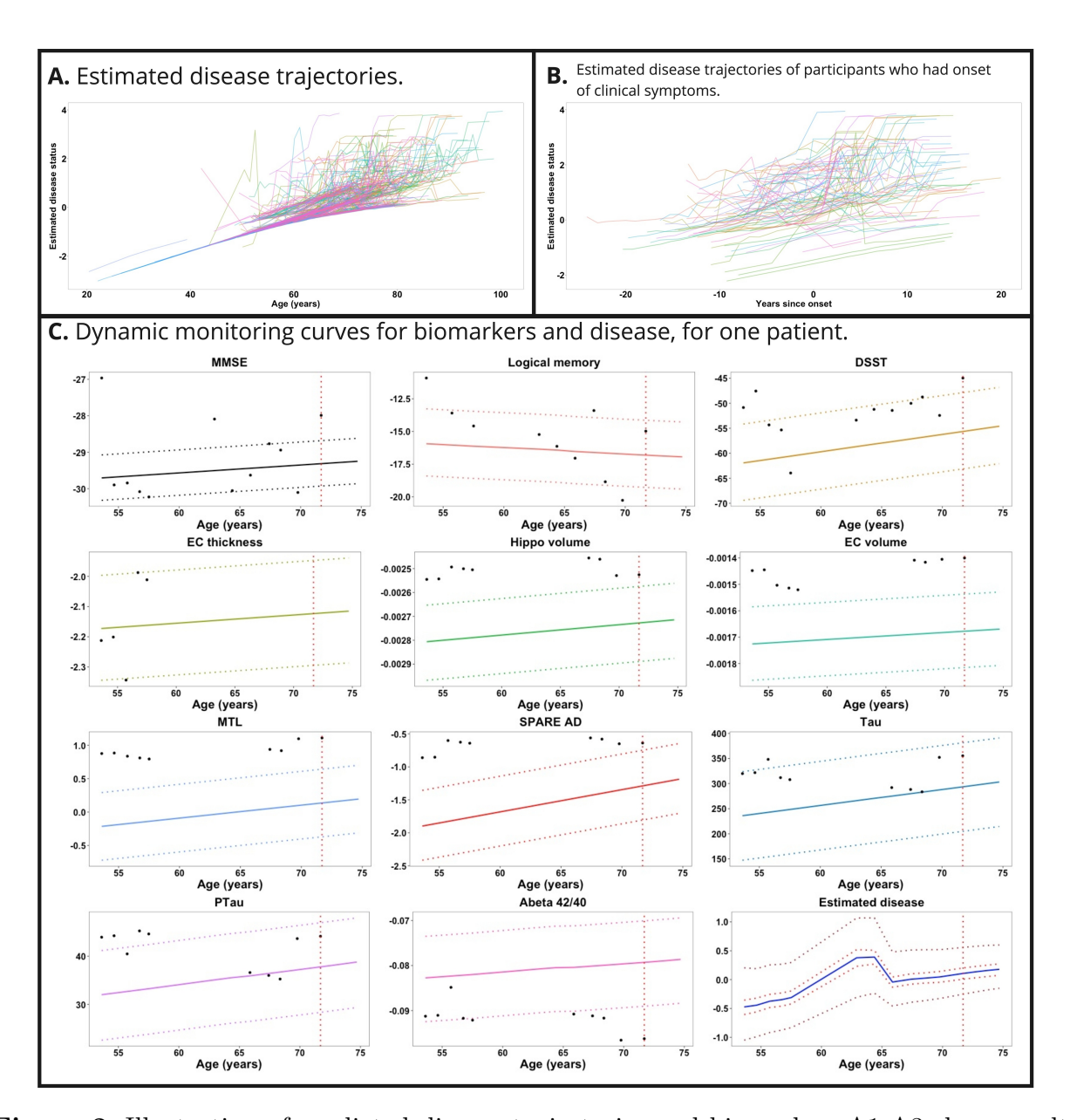


Figure 2: Illustration of predicted disease trajectories and biomarker. A1-A3 show results for BIOCARD; B1-B3 show results for ADNI. A1 and B1 illustrate the estimated biomarker progression curves $f_k(d)$; A2 and B2 illustrate the ordering as shown by the estimated location parameter γ_{k3} ; A3 and B3 illustrate the correlation structures for biomarker error terms.

Table 1: Simulation study summary statistics.

			Scena	rio 1			Scena	rio 2		Scenario 3						
		Bias	ESE	MSE	CP	Bias	ESE	MSE	CP	Bias	ESE	MSE	CP			
Biomarker model parameters																
	β_{k0}	-0.03	2.80	2.61	0.93	-0.02	2.23	1.84	0.90	0.00	2.85	2.61	0.93			
	β_{k1}	0.08	2.17	1.71	0.89	0.07	1.76	1.21	0.83	0.06	2.11	1.71	0.89			
k = 1	β_{k2}	0.02	3.77	3.59	0.93	0.22	2.81	2.54	0.93	-0.07	3.80	3.59	0.93			
$\kappa - 1$	γ_{k2}	1.04	11.20	9.12	0.88	0.53	9.22	6.44	0.83	1.10	10.64	9.14	0.91			
	γ_{k3}	0.01	5.81	5.70	0.95	0.30	4.10	4.04	0.95	0.40	5.76	5.72	0.95			
	σ_k	-0.10	1.31	1.31	0.95	-0.03	0.94	0.92	0.94	-0.10	1.31	1.31	0.95			
	β_{k0}	0.06	3.04	2.61	0.91	-0.10	2.36	1.85	0.89	0.02	2.92	2.62	0.92			
	β_{k1}	0.05	2.22	1.63	0.85	-0.06	1.91	1.16	0.76	0.05	2.24	1.64	0.86			
k = 2	β_{k2}	0.03	3.88	3.55	0.92	0.10	2.99	2.51	0.90	-0.01	3.92	3.55	0.92			
$\kappa = 2$	γ_{k2}	1.44	13.34	11.27	0.90	-0.25	10.96	7.87	0.85	-0.04	13.12	11.17	0.91			
	γ_{k3}	0.26	4.67	4.55	0.95	0.13	3.23	3.22	0.94	0.40	4.64	4.56	0.94			
	σ_k	-0.21	1.30	1.29	0.94	0.03	0.92	0.91	0.95	-0.08	1.36	1.29	0.95			
	β_{k0}	0.08	3.82	2.90	0.86	-0.08	3.20	2.05	0.79	0.07	3.94	2.90	0.85			
	β_{k1}	0.04	2.31	1.84	0.88	-0.09	1.96	1.30	0.81	0.12	2.23	1.83	0.90			
k = 3	β_{k2}	0.26	4.18	3.84	0.93	-0.01	3.19	2.72	0.91	0.08	4.01	3.84	0.95			
$\nu - 2$	γ_{k2}	2.72	38.63	38.02	0.93	2.63	32.10	26.69	0.90	4.89	39.91	38.81	0.94			
	γ_{k3}	0.20	4.53	4.36	0.95	0.05	3.13	3.07	0.95	-0.09	4.69	4.36	0.93			
	σ_k	0.00	1.43	1.39	0.94	0.01	0.99	0.98	0.95	-0.04	1.35	1.39	0.96			
	β_{k0}	-0.20	4.94	3.38	0.83	0.15	4.21	2.39	0.75	-0.11	4.90	3.38	0.81			
	β_{k1}	0.11	2.39	2.22	0.93	-0.04	1.88	1.56	0.90	0.10	2.50	2.21	0.92			
	β_{k2}	0.42	4.66	4.39	0.94	0.07	3.38	3.10	0.94	0.25	4.61	4.39	0.94			
k = 4	γ_{k2}	-6.87	56.85	69.48	0.90	-2.49	50.14	53.04	0.90	-5.02	59.31	70.24	0.89			
	γ_{k3}	-0.45	5.55	5.58	0.94	-0.10	4.11	3.93	0.94	-0.43	5.88	5.57	0.93			
	σ_k	0.07	1.62	1.57	0.93	0.01	1.09	1.11	0.96	-0.04	1.61	1.56	0.94			
	ρ	-0.06	1.00	0.99	0.95	0.03	0.71	0.70	0.95	-0.03	0.99	0.99	0.95			
AD disease progression model parameters																
	α_1	0.22	4.61	4.74	0.96	0.20	3.17	3.35	0.96	0.45	4.70	4.74	0.95			
	α_2	0.16	6.22	6.08	0.94	0.16	4.28	4.30	0.95	0.63	5.91	6.09	0.96			

ESE stands for empirical standard error, and MSE stands for mean standard error. Biases, ESEs, and MSEs are reported in the unit of 10^{-2} .

Table 2: BIOCARD data analysis results
Table 3: ADNI data analysis results

ra	DIC	2. DIC	<i>)</i> ().	ЛΙ	(I	,	uс	wa	an	шу	212	resurts r	aı	,10	0. 11	עו	11.		ıa	ua	a	nai	y 1311.	, 10.	Ju105			
	σ_k	0.67 (0.65, 0.69) 0.92 (0.90, 0.95) 0.89 (0.86, 0.91)	(0.86, 0.92)	(0.92,	(0.89,	(0.84, 0.84, 0.84)	(0.73, 0.00)	$0.63 \ (0.60, 0.65)$ $0.64 \ (0.61, 0.67)$		$ ho_{CSF,2}$	0.10 (-0.04, 0.24)			σ_k	$0.73 \ (0.71, \ 0.75)$ $0.88 \ (0.85, \ 0.90)$	(0.88,	(0.70)	(0.75,	(0.86, 0.86)	0.73 (0.71, 0.74)	(0.75)	0.72 (0.68, 0.76)		$ ho_{CSF,2}$	-0.01 (-0.13, 0.11)			
Progression Curve Parameters Age Ang Ang Gender female Education ** (fixed) ***	7/k3	2.80 (2.71, 2.90) 2.62 (2.42, 2.82) 2.90 (2.73, 3.08) 9.33 (9.07, 9.58)	1.71,	(1.96,	(2.03,	(1.97, 6.00)	1.50 (1.37,	1.46 (1.34, 1.58) $1.00 (0.88, 1.11)$		PMRI,2 PMRI,3 PCSF,1	$0.70 \ (0.63, 0.78)$		γ_{k3}	2.53 (2.41, 2.65) 2.24 (2.13, 2.35)	(2.10)	(1.52,	(1.92,	(1.60,	(T.70)	(0.90,	$0.53 \ (0.41, 0.60)$ $0.25 \ (0.12, 0.39)$		$ ho_{CSF,1}$	0.53 (0.47, 0.59)				
	7k2	5.45 (5.09, 5.80) 2.41 (2.05, 2.77) 2.69 (1.93, 3.45) 5.44 (3.02, 6.05)	(3.35,	(2.78,	(2.93,		7.68,	$5.67 \ (5.24, 6.09)$ $7.99 \ (7.29, 8.68)$			0.72 (0.67, 0.77)		Progression Curve Parameters				γ_{k2}	7.01 (6.38, 7.64) 6.01 (5.12, 6.9)	4.93 (2.59, 7.27)	(6.50,	(2.73,	5.74 (5.08, 6.41)	$4.11 \ (3.63, 4.59)$		6.93 (5.91, 1.88) 6.74 (5.80, 7.67)		$\rho_{MRI,3}$	0.67 (0.61, 0.72)
	$\gamma_{k_1}^*$ (fixed)	5.87 2.83 2.43 5.8	0.74	0.70	1.08	1.60	1.81	2.32			0.45 (0.42, 0.48)			1 Curve Parameters	$\gamma_{k_1}^*$ (fixed)	4.45	2.80				2.35	1.19	1.24		$ ho_{MRI,2}$	0.41 (0.37, 0.46)		
	Education	-0.09 (-0.12, -0.07) -0.10 (-0.14, -0.07) -0.17 (-0.21, -0.14)	0.10 (0.05, 0.14)	-0.01 (-0.06, 0.03)	0.07 (0.03, 0.12)		-0.04 (-0.07, 0.00)	$0.01 \ (-0.02, 0.04)$ $0.00 \ (-0.04, 0.03)$	Other Parameters	$ ho_{MRI,1}$	0.07 (0.05, 0.08)				Education	-0.11 (-0.14, -0.09) -0.26 (-0.29, -0.23)	-0.20 (-0.27, -0.13)	-0.02 (-0.04, 0.01)	0.08 (0.06, 0.11)	$0.01 \ (-0.01, \ 0.04)$	0 (-0.03, 0.02)	.03 (-0.03, -0.01)	0.01 (-0.03, 0.00) -0.09 (-0.13, -0.05)	Other Parameters	$ ho_{MRI,1}$	0.33 (0.32, 0.35)		
	Gender female	-0.11 (-0.16, -0.06) -0.38 (-0.45, -0.31) -0.44 (-0.50, -0.37)	-0.42 (-0.51, -0.33)	$0.11 \ (0.02, 0.21)$	0.38 (0.29, 0.47)	$0.16 \ (0.07, \ 0.25)$	0.06 (-0.01, 0.14)	0.07 (0.01, 0.14) -0.02 (-0.09, 0.05)	0	Pcog	0.15 (0.12, 0.18)		Progression	Gender female	-0.20, -0.10) -0.34, -0.21)		-0.02, 0.08) -	-0.35 (-0.4, -0.31) -0.03 (-0.08, 0.03)	(-0.08, 0.03)	0.37 (0.33, 0.42) 0.07 (-0.02, 0.16)	(-0.02, 0.10)	$0.13 \ (0.03, 0.22)$ $0.03 \ (-0.06, 0.12)$ -0.03	Othe	pcog	0.19 (0.16, 0.22)			
	ApoE-4 carrier	-0.06 (-0.11, 0.00) -0.01 (-0.09, 0.06) 0.02 (-0.05, 0.09) -0.04 (-0.16, 0.08)	-0.03 (-0.12, 0.06)		-0.10 (-0.20, -0.01)	$-0.10 \ (-0.19, -0.01)$	0.02 (-0.06, 0.10)	$0.08 \ (0.01, 0.16)$ $0.60 \ (0.52, 0.67)$			Correlation			ApoE-4 carrier ((0.01, 0.13)	(-0.07, 0.26)	(-0.15, -0.03)	(-0.02, 0.09)	(-0.06, 0.07)	(-0.01, 0.10)	(0.05, 0.25)	(0.13, 0.39) $(0.56, 0.77)$			Correlation 0			
	Age	0.16 (0.14, 0.19) -0.13 (-0.17, -0.08) 0.29 (0.25, 0.33) 0.11 (0.04, 0.18)	0.18 (0.14, 0.23)	0.13 (0.08, 0.18)	0.26 (0.21, 0.31)	$0.40 \ (0.36, \ 0.45)$	$0.20 \ (0.16, 0.24)$	$0.15 \ (0.12, 0.19)$ $0.09 \ (0.06, 0.12)$		ApoE-4 carrier	$0.59\ (0.54,\ 0.64)$			Age	0.14 (0.11, 0.16) 0.07 -0.01 (-0.04, 0.02) 0.02		(0.19, 0.24)	_	(0.14, 0.20)	0.38 (0.35, 0.40) 0.05		(-0.01, 0.10) (-0.02, 0.07)		ApoE-4 carrier	0.39 (0.36, 0.42)			
	Intercept	-0.04 (-0.08, 0.01) 0.10 (0.04, 0.17) 0.20 (0.14, 0.26) -0.15 (-0.26, -0.04)	$0.24 \ (0.17, 0.32)$	-0.05 (-0.12, 0.03)	-0.21 (-0.29, -0.13)	-0.09 (-0.17, -0.02)	-0.24 (-0.30, -0.17)	-0.35 (-0.41, -0.29) -0.48 (-0.54, -0.42)		Age	$0.72\ (0.70,\ 0.75)$			Intercept	-0.03 (-0.07, 0.01) 0.1 0.04 (-0.01, 0.09) -0.0		_		_	$-0.39 \ (-0.44, -0.34) \ 0.39 \ 0.40 \ 0.47 \ 0.39) \ 0.39$	-0.41, -0.32)	-0.34, -0.38 -0.77, -0.61		Age	0.52 (0.48, 0.55) 0.3			
		MMSE LM DSST FC thickness	Hippocampal volume [†]	EC volume	MTL composite score	SPARE AD composite score	Ttau F.	Frau $Aeta$			Disease model				MMSE -0.0 LM 0.0	Γ.	EC thickness -0.2	ume^\dagger		te score	•	Frau -0.40 (A) $A\beta 42/40$ ratio -0.69 (Disease model 0.5			

^{*:} γ_{k1} values are predetermined. †: MRI volumes are adjusted for intracranial volume. Continuous variables were standardized to have mean zero and standard deviation one before model fitting.